nature biotechnology

Systematic identification of allosteric protein-metabolite interactions that control enzyme activity *in vivo*

Hannes Link[1], Karl Kochanowski[1,2] & Uwe Sauer[1]

Recent data suggest that the majority of proteins bind specific metabolites[1,2] and that such interactions are relevant to metabolic and gene regulation[3–5]. However, there are no methods to systematically identify functional allosteric protein-metabolite interactions[4,6]. Here we present an experimental and computational approach for using dynamic metabolite data to discover allosteric regulation that is relevant *in vivo*. By switching the culture conditions of *Escherichia coli* every 30 s between medium containing either pyruvate or ^{13}C-labeled fructose or glucose, we measured the reversal of flux through glycolysis pathways and observed rapid changes in metabolite concentration. We fit these data to a kinetic model of glycolysis and systematically tested the consequences of 126 putative allosteric interactions on metabolite dynamics. We identified allosteric interactions that govern the reversible switch between gluconeogenesis and glycolysis, including one by which pyruvate activates fructose-1,6-bisphosphatase. Thus, from large sets of putative allosteric interactions, our approach can identify the most likely ones and provide hypotheses about their function.

Existing maps of protein-protein[7] and protein-DNA interactions[8] do not comprehensively represent the dynamic molecular interactions that govern phenotypic behavior, in part because interactions between proteins and metabolites are missing. A particular subclass of protein-metabolite interactions is allosteric regulation of metabolic enzymes, which enables instantaneous and reversible modification of catalytic activity[5]. The rapid nature of allosteric regulation renders it the most direct and efficient mechanism to sense concentration changes in small molecules and modulate pathway activity to maintain metabolic homeostasis. *In vitro* biochemical assays have been used for decades to identify allosteric effector metabolites[9], and newer methods have facilitated systematic identification of stable protein-lipid complexes[1,2] and weaker *in vitro* protein-metabolite interactions[10]. However, quantification of the condition- and time-dependent *in vivo* activity of allosteric regulation has not been experimentally possible. *In vivo* relevance has only been inferred through computational modeling, which, for example, has been used to demonstrate how allosteric feedback enhances the stability of red blood cell metabolism[11], enables optimal growth[12], assures robust carbon uptake in *E. coli*[13] and controls pathway usage in *Arabidopsis*[14]. In all cases, one or a few known allosteric interactions were assumed to be functional a priori.

Here we present a quantitative computational and experimental approach to identify allosteric interactions that are relevant *in vivo* without the need for prior knowledge of such interactions. Our approach is based on dynamic metabolomics[15] and ^{13}C isotopic labeling[16] experiments that are analyzed by ensemble modeling[17], where structurally different models represent molecular hypotheses on putative allosteric interactions (**Supplementary Fig. 1**). We use the approach to investigate allosteric interactions that govern the reversible switch from gluconeogenesis to glycolysis in *E. coli* (**Fig. 1a**).

To learn the time scale at which *E. coli* can revert its flux from gluconeogenesis to glycolysis and back, we switched growing batch cultures between the gluconeogenic substrate pyruvate and either of the glycolytic substrates glucose or fructose by using a variant of the filter cultivation method[18] (**Fig. 1b**). Based on initial experiments (data not shown), we traced intracellular fluxes through this bidirectional pathway for 30 s by uniformly ^{13}C-labeled ([U-^{13}C])glucose and [U-^{13}C]fructose experiments. Quantification of isotopic labeling by mass spectrometry[16] revealed that ~50% of the phosphoenolpyruvate (PEP) molecules at the end of this nine-reaction pathway were already labeled within 5 s after switching to [U-^{13}C]glucose (**Fig. 1c**). Although much slower, the labeling profiles during the switch to [U-^{13}C]fructose resemble those of glucose (**Fig. 1d**). Upon switching back to unlabeled pyruvate, the fraction of fully labeled glucose-6-phosphate (G6P) decreases from 80% to 20% within 30 s, demonstrating rapid reversibility of pathway usage. As transcriptional regulation cannot influence fluxes in <30 s, any observed changes in flux in this experimental system are a function of the enzyme kinetics and their allosteric regulation.

To elucidate the role of metabolite regulation for these flux reversals, we determined dynamic concentration changes of 53 central metabolites that were extracted during these 30-s filter experiments (**Supplementary Table 1**). Although all metabolites remained in a stable steady state upon continuous perfusion of filter cultures with pyruvate, they responded instantaneously when cells were switched to a perfusion medium containing glucose or fructose. Sixty-six percent of the measured metabolites varied at least twofold during one of

[1]Institute of Molecular System Biology, ETH Zurich, Zurich, Switzerland. [2]Life Science Zurich PhD Program on Systems Biology, Zurich, Switzerland. Correspondence should be addressed to U.S. (sauer@imsb.biol.ethz.ch).

Received 24 September 2012; accepted 19 December 2012; published online 3 March 2013; doi:10.1038/nbt.2489

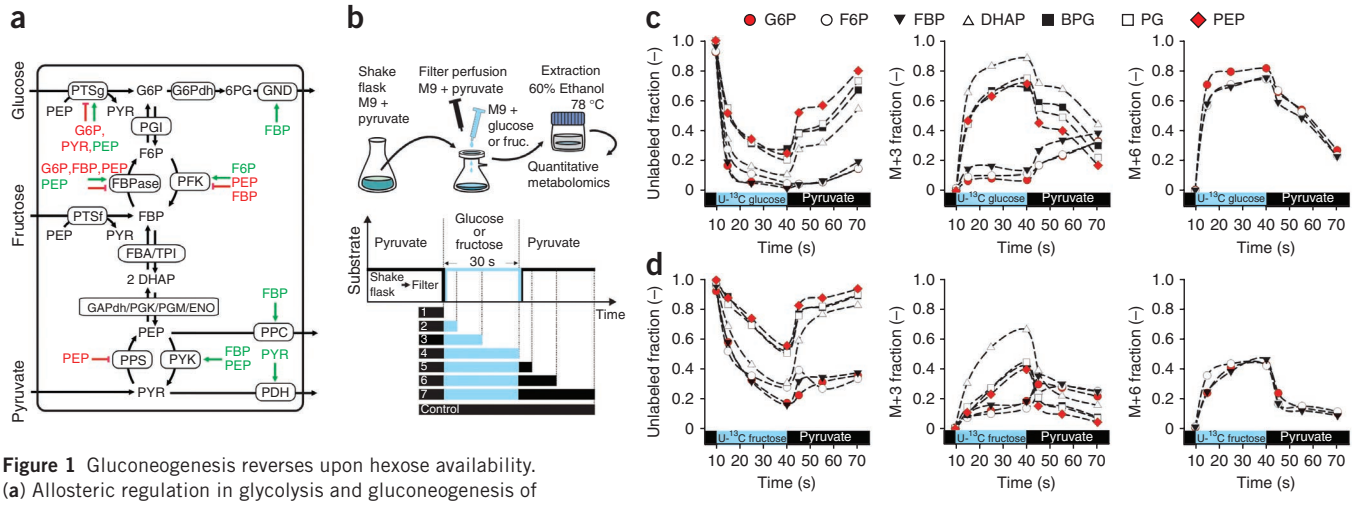

Figure 1 Gluconeogenesis reverses upon hexose availability. (**a**) Allosteric regulation in glycolysis and gluconeogenesis of *E. coli*. Black arrows indicate reactions catalyzed by the boxed enzymes. Reversible reactions are indicated by arrows in both directions. Allosteric interactions between metabolites and enzymes known from literature are indicated by green arrows (activation) and red lines with capped ends (inhibition). (**b**) Experimental setup for fast carbon-source switching. Culture broth from a shake flask is transferred onto a nitrocellulose filter mounted on a vacuum device. Subsequently cells are continuously perfused with medium containing pyruvate and are then switched to a medium containing glucose or fructose. Upon filtration the filter is extracted in hot ethanol and cell extracts are analyzed by ultrahigh performance liquid chromatography–tandem mass spectrometry. Lower panel, perfusion profiles of samples before extraction. Black bars, perfusion with pyruvate medium; blue bars, with either glucose or fructose medium. (**c**,**d**) Fraction of unlabeled metabolites, metabolites labeled with three ^{13}C isotopes (M+3) and six ^{13}C isotopes (M+6) during a pyruvate to U-^{13}C–labeled glucose switch (**c**) and a pyruvate to U-^{13}C–labeled fructose switch (**d**). Dihydroxyacetonephosphate (DHAP), 2,3-bisphosphoglycerate (BPG), 2- and 3-phosphoglycerate (PG), pyruvate (PYR), glucose-specific phosphotransferase system (PTSg), fructose-specific phosphotransferase system (PTSf), phosphoglucoseisomerase (PGI), phosphofructokinase (PFK), fructose-1,6-bisphosphate aldolase (ALD), glyceraldehyde-3-phosphate dehydrogenase (GAPdh), phosphoglucokinase (PGK), phosphoglucomutase (PGM), enolase (ENO), pyruvate kinase (PYK), phosphoenolpyruvate carboxylase (PPC), phosphoenolpyruvate synthetase (PPS), pyruvate dehydrogenase (PDH), glucose-6-phosphate dehydrogenase (G6Pdh) and 6-phosphogluconate dehydrogenase (GND).

the switches (**Fig. 2a** and **Supplementary Fig. 2**). Hexose monophosphates responded most rapidly, reaching almost steady-state levels within 5 s. Most other metabolites also responded instantaneously but did not reach a constant concentration during the 30-s interval. For example, during the glucose switch, the concentration of fructose-1,6-bisphosphate (FBP) increased linearly by over tenfold. After the culture was switched back to pyruvate, nearly all metabolites returned to their initial steady-state levels within 30 s, suggesting that the cells promptly restored their initial state. Notably, *E. coli* maintains energetic homeostasis during the shifts because concentrations of ATP, GTP and their congeners did not change substantially and the energy charge remained constant, as was confirmed by using acidic acetonitrile extraction that prevents nucleotide decomposition[19] (**Supplementary Fig. 3**). All concentration changes were consistent across two independent experiments, illustrating that global metabolite dynamics are robust and that metabolism responds to changing substrates in a reproducible fashion. Although intermediates of the tricarboxylic acid cycle and pentose phosphate pathways exhibited similar profiles (**Supplementary Fig. 2**), intermediates of glycolysis responded very differently to the glucose and fructose switches (**Fig. 2a**).

The rapidly changing metabolite concentrations could cause flux reversal simply by changing the thermodynamic driving forces. According to the second law of thermodynamics, the reaction quotient of substrates and products controls net flux directions and the quotient of reversible reactions must change during the switches. In the lower part of glycolysis, however, small changes within the error of metabolite measurements can tip the favored flux direction[20]. Notably, the ratio of FBP and PEP in the fructose switch did not increase as one would expect if this is the only ratio that controls net flux in the lower part of glycolysis[20], indicating that other factors influence the thermodynamically favored flux direction. Therefore, we applied network-embedded thermodynamic analysis[21] to systematically check flux directions and reaction quotients considering 10% error in metabolite data and other unknown factors, such as the concentration of free phosphate in the cell (**Supplementary Methods**). Changing reaction quotients rendered seven reactions freely reversible, as indicated by free energies that center around zero (**Fig. 2b**). Another eight reactions, however, did not achieve both negative and positive free energies in either switch (**Fig. 2b**). They are therefore thermodynamically irreversible, given the measured metabolite concentration, hence, alternative reactions are required to reverse the flux. For example, phosphofructokinase favors conversion of fructose-6-phosphate (F6P) to FBP, whereas fructose-1,6-bisphosphatase (FBPase) is strongly driven in the opposite direction. As a bidirectional enzyme pair, they render the net flux between F6P and FBP fully reversible, but to achieve flux reversal the activity of phosphofructokinase and FBPase must be actively regulated. Because we can safely assume that enzyme concentrations do not change in the 30-s switches, the reversal of net flux through the pathway must be mediated by active metabolite regulation that could mechanistically be achieved by either active site occupation[20] or by allosteric effectors[4,5].

To obtain a quantitative, mechanistic interpretation of the metabolite dynamics, we developed a kinetic model of glycolysis and the oxidative pentose phosphate pathway. To simplify the model, we did not include the nonoxidative pentose phosphate pathway and assumed that the pathway operates only to supply precursors and redox power for biosynthesis. This assumption is justified because a switch from pyruvate to 1-^{13}C–labeled glucose confirmed that 80–87% of the flux that enters the pentose phosphate pathway is used for biosynthetic purposes (**Supplementary Fig. 4**). The model

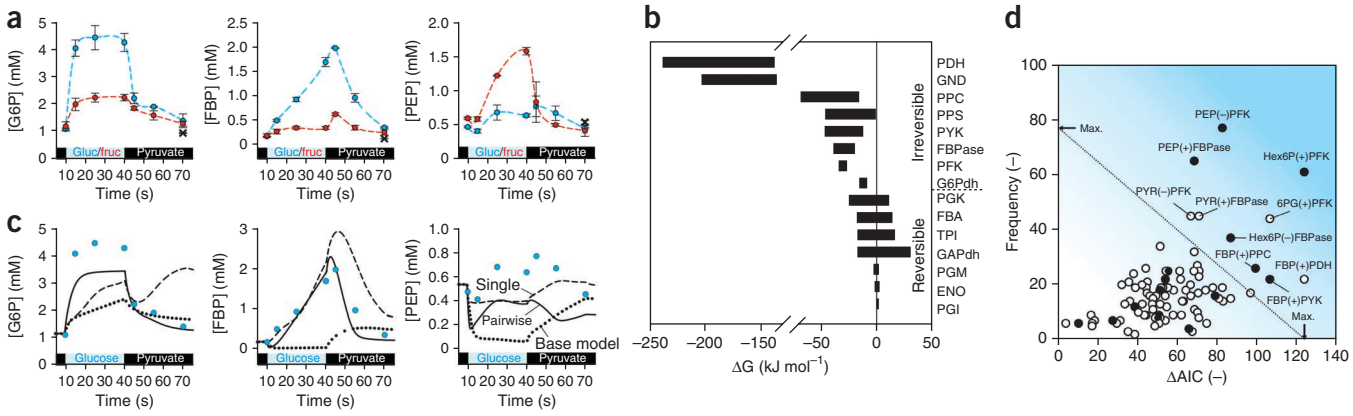

Figure 2 Metabolites regulate flux reversal during carbon source switches. (**a**) Intracellular metabolite concentrations (mmol $L_{cytosol}^{-1}$) during a switch from pyruvate to glucose and back to pyruvate (blue); and a switch from pyruvate to fructose and back to pyruvate (red). A control sample without substrate switching is shown as a cross at 70 s. Error bars indicate the results from two independent experiments and dashed lines are smoothed splines. (**b**) Ranges of free energies during carbon source switches were estimated with network embedded thermodynamic analysis using measured metabolite data and directions of metabolic fluxes (**Supplementary Methods**). Eight reactions are irreversible and seven reactions reversible. (**c**) Metabolite concentrations during the glucose switch were predicted with the base model (dotted line), the best single interaction model (dashed line) and the best pairwise interaction model (solid line). (**d**) Relevance of allosteric interactions based on the frequency of occurrence in good models and the information content of the best model with this interaction (ΔAIC). The dotted line marks 50% of the averaged sum of both criteria. Literature-reported interactions are shown as black dots.

combines mass action and Michaelis-Menten kinetics for reversible and irreversible reactions, respectively. The base model consists of 18 ordinary differential equations, allowing us to simulate the concentration changes of seven metabolites, conversion rates of 14 reactions and ^{13}C-labeling dynamics. Binding constants (K_m) were randomly sampled from an interval of 0.1–10 times around the literature value, and maximum reaction rates (v_{max}) were calculated from flux distributions during steady-state growth on pyruvate (**Supplementary Table 2** and **Supplementary Methods**). Without allosteric regulation, this base model can describe thermodynamic effects by mass action and metabolite regulation by active site occupation. Because the base model without allosteric regulation cannot capture the experimental data of the glucose and fructose switches (**Fig. 2c** and **Supplementary Fig. 5**), allosteric regulation must be necessary for the observed rapid flux switch from gluconeogenesis to glycolysis.

Next, to identify the allosteric effectors that are relevant *in vivo*, we augmented the model with single, allosteric metabolite-enzyme interactions by using a power law term that affects the maximum reaction rates of enzymes. To avoid a bias through pre-existing knowledge, we considered all combinations of allosteric activation and inactivation for the nine irreversible enzymes by all seven metabolites in the model, yielding 126 putative interactions that included 17 known allosteric interactions (**Supplementary Table 3**). We assumed that all reactions identified as reversible are close to equilibrium and are therefore independent of the enzyme activity. The 126 structurally different models, each consisting of the base model plus a single allosteric interaction, were then tested for their capacity to simultaneously describe the glucose and fructose switches. Each model was ranked relative to the base model using the Aikaike information criterion, which is a measure of model information content that accounts for the number of model parameters[22]. Three of the 126 allosteric interactions improved the base model by >40% (**Supplementary Table 4**). Their targets were either phosphofructokinase or FBPase, strongly suggesting that active regulation of this bidirectional enzyme pair was necessary for the flux reversal in upper glycolysis. Notably, the identified effector metabolites were consistent with previously reported observations derived from *in vitro* data that phosphofructokinase is activated by hexose-6-P[23] and inhibited by PEP[24], as well as that FBPase is activated by PEP[25].

To consider pairwise combinations of allosteric interactions, we reduced the complexity by considering the equilibrium reaction metabolite pairs G6P/F6P and FBP/dihydroxyacetone-P as a group because their similar time profiles would not allow us to differentiate between them. This reduced the number of putative interactions from 126 to 90. We then evaluated models with all 3,600 possible pairs of allosteric interactions. Twenty-two percent of pairs increased the capability of the base model to describe the data, but only 2.5% performed better than the best single-interaction model (**Supplementary Fig. 6**). The biological relevance of individual interactions was scored based on, first, how often they occurred in models that improved the base model and, second, the information content of the best model with this interaction (**Fig. 2d** and **Supplementary Table 5**). Overall, ten interactions had an average sum of both criteria >50% (dotted line in **Fig. 2d**), and six of them had been described in previous studies. These six included the three most relevant interactions, which were also identified by the best single-interaction models—namely, activation of phosphofructokinase by hexose-6-P, inhibition of this enzyme by PEP and activation of FBPase by PEP. Additionally, our analysis predicts that both enzymes interact with pyruvate and that phosphofructokinase is activated by 6-phosphogluconate. *In vitro* assays with purified enzyme confirmed the predicted activation of FBPase by pyruvate, which increased activity with saturation-type kinetics >300% and alleviates AMP and G6P inhibition (**Fig. 3a** and **Supplementary Fig. 7**). Consistent with the literature[24], we could not confirm activation of phosphofructokinase by 6-phosphogluconate and inhibition by pyruvate. Although these metabolites are apparently not direct effectors, their high relevance indicates that phosphofructokinase interacts with closely connected metabolites. For example, citrate, which is only two reactions away from pyruvate, is a known inhibitor of phosphofructokinase. Similarly, activation by 6-phosphogluconate indicates positive feedback from other metabolites in the pentose phosphate pathway. Although parameters determined *in vitro* are usually considered not representative *in vivo*, it is notable that the cooperative *in vitro* kinetics of phosphofructokinase

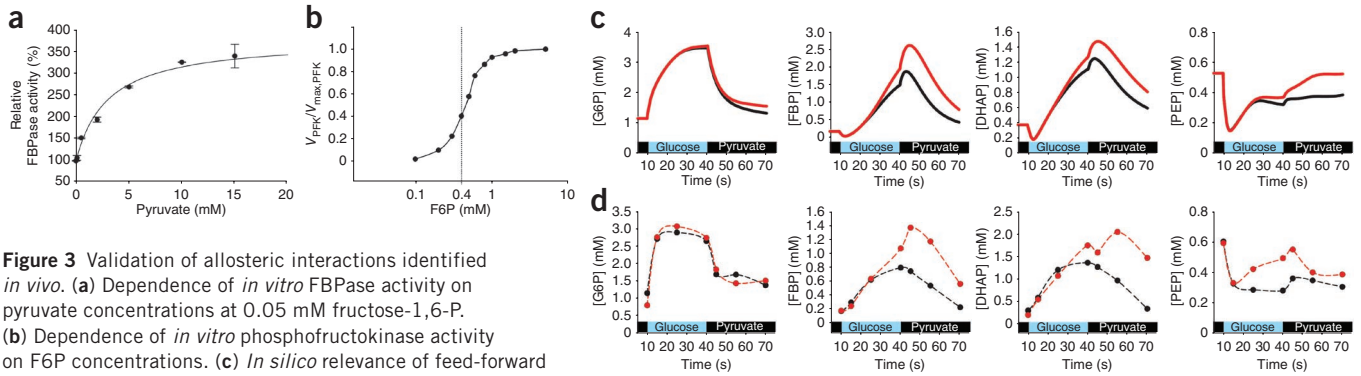

Figure 3 Validation of allosteric interactions identified *in vivo*. (**a**) Dependence of *in vitro* FBPase activity on pyruvate concentrations at 0.05 mM fructose-1,6-P. (**b**) Dependence of *in vitro* phosphofructokinase activity on F6P concentrations. (**c**) *In silico* relevance of feed-forward activation of lower glycolysis by FBP. The black lines show time profiles of intracellular metabolite concentrations during the glucose switch that were simulated with a model including seven allosteric interactions. The red line shows simulations when removing allosteric regulation of pyruvate kinase by FBP from this model. (**d**) *In vivo* relevance of feed-forward activation of lower glycolysis by FBP. Intracellular metabolite concentrations during a glucose switch with *E. coli* lacking the *pykF* gene and carrying plasmids with genes encoding the native (black) and a FBP-insensitive pyruvate kinase (red). Dashed lines are smoothed splines.

toward the substrate F6P shows the steepest part of the curve ($K_{0.5}$) at a concentration of 0.4 mM, precisely the *in vivo* concentration during growth on pyruvate (**Fig. 3b** and **Supplementary Fig. 8**). G6P had no effect on phosphofructokinase activity.

In contrast to single-interaction models, the pairwise models also identified FBP activation of lower glycolysis enzymes to be relevant. Although FBP activation of pyruvate kinase[26] and PEP carboxylase[27] was already known, to our knowledge FBP activation of pyruvate dehydrogenase has not been described. As this feed-forward activation of lower glycolysis by FBP is not strictly necessary for flux switching, we simulated the glucose switch with a model containing the seven interactions identified *in vivo* that were also confirmed *in vitro* (**Fig. 3c**). The seven allosteric interactions are G6P activation and PEP inhibition of phosphofructokinase; pyruvate activation, PEP activation and G6P inhibition of FBPase; FBP activation of pyruvate kinase; and FBP activation of PEP carboxylase. Removing FBP activation of pyruvate kinase in this model predicts accumulation of FBP and dihydroxyacetone-P upon influx of glucose and a limited capability to switch back to the initial steady state on pyruvate. To verify this prediction, we used a strain of *E. coli* in which *pykF* was deleted to express either the wild-type pyruvate kinase or a mutant pyruvate kinase rendered insensitive to FBP by a point mutation in the FBP-binding site[26]. Consistent with the model's prediction, steady-state concentrations and the dynamic profiles of G6P and F6P were similar in both strains, but after 30 s much higher peak concentrations of FBP and dihydroxyacetone-P were observed in the strain expressing the mutant enzyme (**Fig. 3d**). Both model and data show that reduced sensitivity of pyruvate kinase to FBP prolongs the time needed to restore steady-state concentrations of FBP and dihydroxyacetone-P upon switching back to pyruvate. Consistently, all good pairwise models suggest that FBP feed-forward activation plays a pivotal role in the maintenance of metabolite concentration homeostasis and allows for a rapid return to the pyruvate steady state. Complete loss of FBP activation of lower glycolysis would presumably cause a drastic accumulation of glycolytic intermediates and preclude a return to the initial steady state.

Without a priori information on allosteric regulation, we identified allosteric interactions active *in vivo* and generated hypotheses about their functional importance. Of nine putative allosteric targets, phosphofructokinase occurred most frequently in the pairwise interaction models (**Fig. 2d**), suggesting that it is the most relevant enzyme under the experimental conditions used. Fructose-6-P activated phosphofructokinase in a cooperative manner within 5 s after glucose addition. The concentration profile of F6P shows that cooperativity occurred *in vivo* at the same concentration that we determined *in vitro* using purified phosphofructokinase (**Supplementary Fig. 2** and **Fig. 3b**). The concentration of PEP was relatively constant during the switch to glucose, suggesting that the role of PEP inhibition of phosphofructokinase is to adjust glycolytic PEP formation to the multiple PEP-consuming reactions, including glucose uptake by means of the phosphotransferase system. In the fructose switch, however, rapidly increasing PEP concentrations (**Fig. 2a**) inhibited phosphofructokinase and thereby compensated for the effect of increasing hexose-6-P concentrations that would otherwise activate phosphofructokinase to further increase glycolytic flux. Transiently increasing FBP concentrations maintain metabolite concentration homeostasis by feed-forward activation of lower glycolytic enzymes. The same interactions are active when switching back to pyruvate metabolism because the immediate drop of F6P inactivates phosphofructokinase and the FBP feed-forward regulation ensures that concentrations return rapidly to their initial state.

Under gluconeogenic conditions, FBPase is normally inactive and requires allosteric activation[25] that can be achieved by multiple, and potentially redundant, activators such as citrate or PEP. The newly identified allosteric activation of FBPase through pyruvate is probably required for full activation of FBPase during growth on pyruvate and potentially similar carbon sources such as lactate. It is tempting to speculate that this allosteric interaction could also be present in eukaryotes, where pyruvate is a key metabolite at the interface of cytosolic and mitochondrial metabolism.

The method we have described enables systematic mapping of allosteric interactions with physiological relevance under specific conditions, which will facilitate our understanding of metabolic feedback regulation and its role in cellular homeostasis. The key step of our method is the use of dynamic metabolite data to discriminate between ensembles of structurally different models[17], each representing a putative allosteric regulation mechanism. This requires computational models that capture the most relevant components and processes, but statistical sampling can, to some extent, compensate for model uncertainties such as missing binding constants or unmeasured concentrations and reaction rates. Among large sets of putative allosteric interactions, our method identifies the most likely and provides hypotheses about their function. Validation of the functional importance requires mutant enzymes as shown here for pyruvate kinase or direct approaches that focus on single interactions,

as recently demonstrated for regulation of PEP carboxylase[28]. Besides discovering allosteric regulation in uncharacterized organisms and pathways, the approach we have outlined is, in principle, also applicable to other perturbations that affect metabolite dynamics by modulating the activity of one or a few enzymes. For example, the approach could be applied to small-molecule inhibitors to identify their metabolic targets and whether they act as homotropic or heterotropic allosteric regulators.

METHODS

Methods and any associated references are available in the online version of the paper.

Note: Supplementary information is available in the online version of the paper.

ACKNOWLEDGMENTS

We thank E. Zamora-Sillero, L. Gerosa, M. Zampieri and R. Milo for discussions. This work was supported by Deutsche Forschungsgemeinschaft grant Li 1993/1-1.

AUTHOR CONTRIBUTIONS

H.L. co-wrote the manuscript, performed and conceived experiments and computational analysis, K.K. performed experiments and constructed strains and edited the final draft, U.S. co-wrote the manuscript and directed the project.

COMPETING FINANCIAL INTERESTS

The authors declare no competing financial interests.

1. Li, X., Gianoulis, T.A., Yip, K.Y., Gerstein, M. & Snyder, M. Extensive *in vivo* metabolite-protein interactions revealed by large-scale systematic analyses. *Cell* **143**, 639–650 (2010).
2. Gallego, O. *et al.* A systematic screen for protein-lipid interactions in *Saccharomyces cerevisiae*. *Mol. Syst. Biol.* **6**, 430 (2010).
3. Hilser, V.J. An ensemble view of allostery. *Science* **327**, 653–654 (2010).
4. Lindsley, J.E. & Rutter, J. Whence cometh the allosterome? *Proc. Natl. Acad. Sci. USA* **103**, 10533–10535 (2006).
5. Gerosa, L. & Sauer, U. Regulation and control of metabolic fluxes in microbes. *Curr. Opin. Biotechnol.* **22**, 566–575 (2011).
6. Heinemann, M. & Sauer, U. Systems biology of microbial metabolism. *Curr. Opin. Microbiol.* **13**, 337–343 (2010).
7. Petschnigg, J., Snider, J. & Stagljar, I. Interactive proteomics research technologies: recent applications and advances. *Curr. Opin. Biotechnol.* **22**, 50–58 (2011).
8. Stormo, G.D. & Zhao, Y. Determining the specificity of protein-DNA interactions. *Nat. Rev. Genet.* **11**, 751–760 (2010).
9. Scheer, M. *et al.* BRENDA, the enzyme information system in 2011. *Nucleic Acids Res.* **39**, D670–D676 (2011).
10. Orsak, T. *et al.* Revealing the allosterome: systematic identification of metabolite–protein interactions. *Biochemistry* **51**, 225–232 (2012).
11. Grimbs, S., Selbig, J., Bulik, S., Holzhütter, H.-G. & Steuer, R. The stability and robustness of metabolic states: identifying stabilizing sites in metabolic networks. *Mol. Syst. Biol.* **3**, 146 (2007).
12. Goyal, S., Yuan, J., Chen, T., Rabinowitz, J.D. & Wingreen, N.S. Achieving optimal growth through product feedback inhibition in metabolism. *PLoS Comput. Biol.* **6**, e1000802 (2010).
13. Kremling, A., Bettenbrock, K. & Gilles, E.D. A feed-forward loop guarantees robust behavior in *Escherichia coli* carbohydrate uptake. *Bioinformatics* **24**, 704–710 (2008).
14. Curien, G. *et al.* Understanding the regulation of aspartate metabolism using a model based on measured kinetic parameters. *Mol. Syst. Biol.* **5**, 271 (2009).
15. Buescher, J.M., Moco, S., Sauer, U. & Zamboni, N. Ultrahigh performance liquid chromatography-tandem mass spectrometry method for fast and robust quantification of anionic and aromatic metabolites. *Anal. Chem.* **82**, 4403–4412 (2010).
16. Ruehl, M. *et al.* Collisional fragmentation of central carbon metabolites in LC-MS/MS increases precision of 13C metabolic flux analysis. *Biotechnol. Bioeng.* **109**, 763–771 (2012).
17. Kuepfer, L., Peter, M., Sauer, U. & Stelling, J. Ensemble modeling for analysis of cell signaling dynamics. *Nat. Biotechnol.* **25**, 1001–1006 (2007).
18. Yuan, J., Bennett, B.D. & Rabinowitz, J.D. Kinetic flux profiling for quantitation of cellular metabolic fluxes. *Nat. Protoc.* **3**, 1328–1340 (2008).
19. Rabinowitz, J.D. & Kimball, E. Acidic acetonitrile for cellular metabolome extraction from *Escherichia coli*. *Anal. Chem.* **79**, 6167–6173 (2007).
20. Bennett, B.D. *et al.* Absolute metabolite concentrations and implied enzyme active site occupancy in *Escherichia coli*. *Nat. Chem. Biol.* **5**, 593–599 (2009).
21. Kümmel, A., Panke, S. & Heinemann, M. Putative regulatory sites unraveled by network-embedded thermodynamic analysis of metabolome data. *Mol. Syst. Biol.* **2**, 0034 (2006).
22. Turkheimer, F.E., Hinz, R. & Cunningham, V.J. On the undecidability among kinetic models: from model selection to model averaging. *J. Cereb. Blood Flow Metab.* **23**, 490–498 (2003).
23. Johnson, J.L. & Reinhart, G.D. MgATP and fructose 6-phosphate interactions with phosphofructokinase from *Escherichia coli*. *Biochemistry* **31**, 11510–11518 (1992).
24. Blangy, D., Buc, H. & Monod, J. Kinetics of the allosteric interactions of phosphofructokinase from *Escherichia coli*. *J. Mol. Biol.* **31**, 13–35 (1968).
25. Hines, J.K., Fromm, H.J. & Honzatko, R.B. Novel allosteric activation site in *Escherichia coli* fructose-1,6-bisphosphatase. *J. Biol. Chem.* **281**, 18386–18393 (2006).
26. Valentini, G. *et al.* The allosteric regulation of pyruvate kinase. A site-directed mutagenesis study. *J. Biol. Chem.* **275**, 18145–18152 (2000).
27. Wohl, R.C. & Markus, G. Phosphoenolpyruvate carboxylase of *Escherichia coli*. Purification and some properties. *J. Biol. Chem.* **247**, 5785–5792 (1972).
28. Xu, Y.-F. *et al.* Ultrasensitive regulation of anapleurosis via allosteric activation of PEP carboxylase. *Nat. Chem. Biol.* **8**, 562–568 (2012).

ONLINE METHODS

Strains and media. *E. coli* BW 25113 was cultivated in 500-mL shake flasks with M9 minimal medium[29] containing 5 g L^{-1} pyruvate. The perfusion medium for substrate switches was 37 °C M9 medium containing either 5 g L^{-1} sodium pyruvate, 5 g L^{-1} glucose or 5 g L^{-1} fructose. The pH was adjusted to that of the culture before the switch. Strain PykF was constructed by P1 phage transduction of the kanamycin marker from the Keio collection strain JW1666 into the BW 25113 background[30], followed by excision of the kanamycin marker. Plasmid pTrc99KK was derived from pTrc99a using PCR (P1: CGGGATCCTCTAGAGTCGACCTGCAGGC, P2:CGGGATCC GCCTCGAGTCTGTTTCCTGTGTGAAATTG). pTrc99KK-*pykF* expression plasmids with a N-terminal 6xHis-tag were constructed using PCR (P1: CGGGATCCATGCATCATCATCATCATCATATGAAAAAGACCAAA ATTGTTTGCAC, P2: CGAAGCTTTTAC-AGGACGTGAACAGATG), and a FBP-insensitive pTrc99KK-*pykF*(K382Q) plasmid was constructed using site-directed mutagenesis (P: GCTACTCAGGGCGGTCAATCTGCTCGCG CAGTA) as described previously[26].

Substrate switches. Shake flask cultures were grown exponentially to an optical density at 600 nm between 0.4 and 0.6, and 2-ml culture aliquots were vacuum-filtered on a 0.45 µm pore size nitrocellulose filter (Millipore) and perfused for 10 s with M9 medium containing 5 g L^{-1} pyruvate at 37 °C. Substrate switches were realized by changing the perfusion solution to M9 medium containing 5 g L^{-1} glucose or fructose (**Fig. 1b**). For labeling experiments the M9 medium contained 5 g L^{-1} [U-^{13}C]glucose or [U-^{13}C]fructose (^{13}C ≥ 99%, Cambridge Isotope Laboratories).

Metabolite measurements. After washing samples with the according washing profile, the filter was immediately transferred for extraction into 4 ml of 60:40 ethanol/water kept at 78 °C for 2 min. Alternatively cold extraction with 40:40:20 acetonitrile/methanol/water with 0.1 M formic acid was used[19]. Determination of absolute metabolite concentration in the extract was performed as described recently[15].

Kinetic modeling. MATLAB 2011b was used for all calculations and the kinetic model was implemented in Simulink. The model is detailed in **Supplementary Methods**.

29. Fischer, E. & Sauer, U. Metabolic flux profiling of *Escherichia coli* mutants in central carbon metabolism using GC-MS. *Eur. J. Biochem.* **270**, 880–891 (2003).
30. Baba, T. *et al.* Construction of *Escherichia coli* K-12 in-frame, single-gene knockout mutants: the Keio collection. *Mol. Syst. Biol.* **2**, 0008 (2006).

doi:10.1038/nbt.2489